

Multispectral digital microscopy for *in vivo* monitoring of oral neoplasia in the hamster cheek pouch model of carcinogenesis

**Sun Young Park, Tom Collier, Jesse Aaron, Mia K. Markey,
and Rebecca Richards-Kortum**

*Department of Biomedical Engineering, Univ. of Texas, Austin, TX 78712 USA
Tel: (512) 471-3619
sunyoung@mail.utexas.edu, kortum@mail.utexas.edu*

Konstantin Sokolov

*Department of Imaging Physics, UT M.D. Anderson Cancer Center, Houston, TX 77030 USA
Tel: (512) 471-7440
konstantin.sokolov@engr.utexas.edu*

Nick Mackinnon, Calum MacAulay

*Department of Cancer Imaging, British Columbia Cancer Center, Vancouver, BC V5Z 4E6 Canada
Tel: (604) 877-6000
nmackinn@bccancer.bc.ca, cmacula@bccancer.bc.ca*

Lezlee Coghlan

*UT M.D. Anderson Cancer Center, Science Park – Research division, Smithville, TX 78957 USA
Tel: (512) 321-8553
lcoghlan@mdanderson.org*

Andrea Milbourne and Michele Follen

*Department of Gynecologic Oncology, UT M.D. Anderson Cancer Center, Houston, TX 77030 and the Department of
Obstetrics, Gynecology and Reproductive Sciences, UT Health Science Center-Houston, Houston, TX 77030
Tel: (713) 745-2564
amilbour@mdanderson.org, mfolllen@mdanderson.org*

Abstract: In this study we use a multi-spectral digital microscope (MDM) to measure multi-spectral auto-fluorescence and reflectance images of the hamster cheek pouch model of DMBA (dimethylbenz[α]anthracene)-induced oral carcinogenesis. The multi-spectral images are analyzed both in the RGB (red, green, blue) color space as well as in the YCbCr (luminance, chromatic minus blue, chromatic minus red) color space. Mean image intensity, standard deviation, skewness, and kurtosis are selected as features to design a classification algorithm to discriminate normal mucosa from neoplastic tissue. The best diagnostic performance is achieved using features extracted from the YCbCr space, indicating the importance of chromatic information for classification. A sensitivity of 96% and a specificity of 84% were achieved in separating normal from abnormal cheek pouch lesions. The results of this study suggest that a simple and inexpensive MDM has the potential to provide a cost-effective and accurate alternative to standard white light endoscopy.

©2005 Optical Society of America

OCIS codes: (170.6280) Spectroscopy, fluorescence and luminescence; (170.6510) Spectroscopy, tissue diagnostics; (100.5010) Pattern recognition and feature extraction

References and links

1. J.C. Zenklusen, S.L. Stockman, S.M. Fischer SM, C.J. Conti, I.B. Gimenez-Conti, "Transforming growth factor-beta 1 expression in Syrian hamster cheek pouch carcinogenesis," *Mol. Carcinog.* **9**, 10-16 (1994).
2. I.B. Gimenez-Conti, D.M. Shin, A.B. Bianchi, D.R. Roop, W.K. Hong, C.J. Conti, T.J. Slaga, "Changes in keratin expression during 7,12-dimethylbenz[a]anthracene-induced hamster cheek pouch carcinogenesis," *Cancer Res.* **50**, 4441-4445 (1990).
3. L. Coghlan, U. Utzinger, R. Richards-Kortum, C. Brookner, A. Zuluaga, I. Gimenez-Conti, M. Follen-Mitchell, "Fluorescence spectroscopy of epithelial tissue throughout the dysplasia-carcinoma sequence in an animal model: spectroscopic changes precede morphologic changes," *Lasers Surg. Med.* **29**, 1-10 (2001).
4. L. Coghlan, U. Utzinger, R. Drezek, D. Heintzelman, A. Zuluaga, C. Brookner, R. Richards-Kortum, "Optimal fluorescence excitation wavelengths for detection of squamous intra-epithelial neoplasia: results from an animal model," *Opt. Express* **7**, 436-445 (2000).
5. E. Sevick-Muraca and R. Richards-Kortum, "Quantitative optical spectroscopy for tissue diagnosis," *Ann Rev Phys. Chem.* **47**, 555-606 (1996).
6. G.A. Wagnieres, W.M. Star, and B.C. Wilson, "In vivo fluorescence spectroscopy and imaging for oncological applications," *Photochem. Photobiol.* **68**, 603-32 (1998).
7. H. Stepp, R. Sroka, R. Baumgartner, "Fluorescence endoscopy of gastrointestinal diseases: basic principles, techniques, and clinical experience," *Endoscopy* **30**, 379-86 (1998).
8. S.B. Cantor, M. Follen-Mitchell, G. Tortolero-Luna, C. Bratka, D. Bodurka, R. Richards-Kortum, "Cost-effectiveness analysis of diagnosis and management of cervical squamous intraepithelial lesions," *Obstet. Gynecol.* **91**, 270-277 (1998).
9. A.R. Gillenwater, R. Jacob, R. Ganeshappa, B. Kemp, A.K. El-Naggar, J.L. Palmer, G. Clayman, M. Follen-Mitchell, and R. Richards-Kortum, "Noninvasive diagnosis of oral neoplasia based on fluorescence spectroscopy and native tissue autofluorescence," *Arch. Otolaryngol.*, 1251-1258 (1998).
10. N. Ramanujam, M. Follen-Mitchell, A. Mahadevan-Jansen, S. Thomsen, G. Staerker, A. Malpica, T. Wright, N. Atkinson and R. Richards-Kortum, "Cervical precancer detection using multivariate statistical algorithm based on laser-induced fluorescence spectra at multiple excitation wavelengths," *Photochem. Photobiol.* **64**, 720-735 (1996).
11. A. Agrawal, U. Utzinger, C. Brookner, C. Pitris, M. Follen-Mitchell, R. Richards-Kortum, "Fluorescence spectroscopy of the cervix: influence of acetic acid, cervical mucus, and vaginal medications," *Lasers Surg. Med.*, **25**, 237-49 (1999).
12. A. Gillenwater, R. Jacob, R. Ganeshappa, B. Kemp, A.K. El-Naggar, J.L. Palmer, G. Clayman, M. Follen-Mitchell, and R. Richards-Kortum, "Noninvasive diagnosis of oral neoplasia based on fluorescence spectroscopy and native tissue autofluorescence," *Arch. Otolaryngol.* **124**, 1251-1258 (1998).
13. J.K. Dhingra, X. Zahng, K. McMillan, S. Kabani, R. Manoharan, I. Itzkan, M.S. Feld, S.M. Sharpshay, "Diagnosis of head and neck precancerous lesions in an animal model using fluorescence spectroscopy," *Laryngoscope* **108**, 471-475 (1998).
14. C.Y. Wang, T. Tsai, H.C. Chen, S.C. Chang, C.T. Chen, and C.P. Chiang, "Autofluorescence spectroscopy for in vivo diagnosis of DMBA-induced hamster buccal pouch pre-cancers and cancers," *J. Oral Pathol. Med.* **32**, 18-24 (2003).
15. N. Vengadesan, P. Aruna, and S. Ganesan, "Characterization of native fluorescence from DMBA-treated hamster cheek pouch buccal mucosa for measuring tissue transformation," *Br. J. Cancer* **77**, 391-5 (1998).
16. C.T. Chen, H.K. Chiang, S.N. Chow, C.Y. Wang, Y.S. Lee, J.C. Tsai, C.P. Chiang, "Autofluorescence in normal and malignant human oral tissues and in DMBA-induced hamster buccal pouch carcinogenesis," *J. Oral Pathol. Med.* **27**, 470-474 (1998).
17. D.L. Heintzelman, U. Utzinger, et al., "Optimal excitation wavelengths for in vivo detection of oral neoplasia using fluorescence spectroscopy," *Photochem. Photobiol.* **72**, 103-113 (2000).
18. M.G. Muller, T.A. Valdez, I. Georgakoudi, V. Backman, C. Fuentes, S. Kabani, N. Laver, Z. Wang, C.W. Boone, R.R. Dasari, S.M. Shapshay, and M.S. Feld, "Spectroscopic detection and evaluation of morphologic and biochemical changes in early human oral carcinoma," *Cancer* **97**, 1681-1692 (2003).
19. J.M. Benavides, S. Chang, S.Y. Park, R. Richards-Kortum, N. MacKinnon, C. MacAulay, A. Milbourne, A. Malpica, M. Follen, "Multispectral digital colposcopy for the in vivo detection of cervical cancer", *Opt. Express* **11**, 1223:1236(2003).
20. V. Bhaskaran, K. Konstantinides, *Image and video compression standards algorithms and architectures* (Kluwer Academic Publishers, USA, 1999).
21. S.K. Chang, M. Follen, A. Malpica, U. Utzinger, S. Gtaerker, D. Cox, N. Atkinson, C. MacAulay, R. Richards-Kortum, "Optimal excitation wavelengths for discrimination of cervical neoplasia," *IEEE Trans. Biomed. Eng.* **49**, 1102-1111 (2002).
22. B.W. Fei, Z.H. Lee, D.T. Boll, J.L. Duerk, D.B. Sodee, J.S. Lewin, D.L. Wilson, "Registration and fusion of SPECT, high-resolution MRI, and interventional MRI for thermal ablation of prostate cancer," *IEEE Trans. Nucl. Science* **51**: 177-183 Part 1(2004).
23. F. Maes, A. Collignon, D. Vandermeulen, G. Marchal, P. Seutens, "Multimodality image registration by maximization of mutual information," *IEEE Trans. Med. Imaging* **16**, 187-198 (1997).
24. R. Hsu, M. Abdel-Mottaleb, and A. K. Jain, "Face detection in color images," *IEEE Trans. Patt. Anal. Mach. Intell.* **24**: 696-706 (2002).
25. O.D. Richard, E.H. Peter, G.S. David, *Pattern Classification* (John Wiley & Sons, Inc., 2001).
26. A. Bera, C. Jarque, "Efficient tests for normality, heteroskedasticity and serial independence of regression residuals: Monte Carlo evidence," *Econo. Letter* **7**: 313-318 (1981).

1. Introduction

Animal models are of great importance in attempting to better understand the natural history and molecular biology of carcinogenesis. The hamster cheek pouch carcinogenesis model is a well-known and well-characterized animal model of human oral cancer and squamous cell carcinomas (SCC) [1, 2]. The model uses chronic treatments of the cheek pouch with DMBA. Histologically, the 16-week treatment protocol pushes the epithelial lining of the cheek pouch through stages of inflammation, hyperplasia, dysplasia, and both benign and malignant tumor formation [3,4]. Epithelial hyperplasia develops after only a few treatments with DMBA. Dysplastic lesions, resembling human premalignant lesions, are seen after 6-8 weeks of treatment. After about 10 weeks, papillomas and carcinomas begin to appear [1].

Fluorescence spectroscopy is a promising new technology for *in vivo* detection of epithelial dysplasia [5-12]. A number of clinical trials of fluorescence spectroscopy have been performed in humans, demonstrating diagnostic potential in a variety of organ sites. To fully understand the diagnostic potential of fluorescence spectroscopy for early lesion detection, it would be useful to interrogate a single site throughout the entire dysplasia-carcinoma sequence. Obviously, ethical considerations prevent using fluorescence spectroscopy to follow the natural history of carcinogenesis *in vivo* in patients. As an alternative, several *in vivo* animal studies have been performed using fluorescence spectroscopy to follow the development of neoplasia in the hamster cheek pouch model [3, 4, 13]. Wang [14] measured autofluorescence emission spectra *in vivo* from DMBA-induced pre-cancers and early cancers in the hamster cheek pouch at 330 nm excitation. In the study, Wang showed results indicating that the autofluorescence spectroscopy technique is a useful diagnostic tool for *in vivo* diagnosis of oral pre-cancers and cancers in the DMBA-induced hamster cheek pouch carcinogenesis model. Vengadesan [15] studied native fluorescence spectra using the DMBA-induced hamster cheek pouch carcinogenesis model at 405 nm excitation, and characterized the native fluorescence of endogenous porphyrin and other fluorophores. Coghlan [3] showed that neoplastic lesions in the DMBA-induced hamster cheek pouch carcinogenesis model exhibit characteristic red fluorescence between 630-640 nm emission at 410 nm excitation, attributed to porphyrins. Coghlan also demonstrated that fluorescence spectroscopy could identify squamous intra-epithelial neoplasias with high sensitivity and specificity at optimal fluorescence excitation wavelengths of 350-370 nm and 400-450 nm [4]. Similar results were obtained in fluorescence measurements of early cancers of the human oral cavity in several clinical trials [5, 16-18]. Heintzelman [17] determined optimal excitation-emission wavelength combinations for *in vivo* identification of oral cavity neoplasia and showed that the optimal excitation wavelengths for detection of human oral neoplasia were 350, 380 and 400 nm. Muller [18] analyzed fluorescence data from oral tissue for the diagnosis of early oral carcinoma using trimodal spectroscopy. The results demonstrated the method is a highly sensitive and specific technique for tissue abnormality diagnosis.

Previous studies in the hamster cheek pouch model system have used a fiber optic probe to obtain emission spectra from a small area of tissue, typically with a radius less than 2 mm. Due to this limitation, it is difficult to screen the whole field at risk and to determine whether fluorescence can be used to effectively delineate the borders of neoplastic lesions. Recently, an MDM, which is a two dimensional, multispectral imaging system, has been developed and applied for the *in vivo* detection of cervical neoplasia [19]. Unlike the fiber optic spectroscopy approaches, this device has the advantage of being able to assess the entire field at risk.

In this study, we use the MDM to acquire multispectral fluorescence and reflectance images of the entire field at risk. The hamster cheek pouch model is adopted for the study since it provides a highly predictable model of neoplasia which can be studied over a short period of time. Images acquired at different time points in the study are analyzed to visualize and classify neoplastic lesions. In order to separate the chromatic information from the intensity information, the original data acquired in the RGB color space is transformed to the

YCbCr color space. Various statistical parameters are extracted from the images such as the mean pixel value in each image channel, standard deviation, skewness, and kurtosis. A linear discriminant classification algorithm based on the Mahalanobis distance measure [20] is developed and tested using a cross validation technique. Results show that the chromatic information is an important parameter to identify the presence of neoplasia with high sensitivity and specificity.

2. Materials and methods

2.1 Multispectral digital microscope (MDM)

In order to assess the entire field at risk, an MDM was developed to measure multispectral reflectance images with white light illumination and autofluorescence images at 345 nm and 440 nm excitation. We chose these two excitation wavelengths based on an analysis of the two most useful wavelengths for diagnosis of cervical intraepithelial neoplasia from our previous hamster study and a large *in vivo* diagnostic trial of point spectroscopy [3,4,21].

The MDM is composed of a light source, a standard colposcope, and a video rate color CCD camera with a frame grabber [19]. A system diagram of the MDM system is shown in Fig. 1(a). The MDM was built around a commercially available, tilt-stand colposcope (Model 1DL, Leisegang, Germany). This colposcope produces stereoscopic vision at 7.5X magnification. The original halogen lamp of the colposcope was removed to accommodate a fiber optic light guide, coupled to a Xenon arc lamp, which provides broadband illumination for reflectance imaging and monochromatic illumination for fluorescence imaging. Monochromatic light for fluorescence excitation is produced using 20 nm bandwidth band-pass filters (Chroma Technology Corp., Rockingham, VT) centered at 345 nm and 440 nm excitation enclosed in a motorized filter wheel. The optical density of each band-pass filter was at least 4 in the out of band regions. Long pass filters (Omega Optical Inc., Brattleboro, VT) at 388 nm and 468 nm block scattered excitation light during collection of fluorescence images. Each long-pass filter has an optical density of at least 5 below the cut-on wavelength. The reflectance and the fluorescent light are captured and filtered using a commercially available video rate color charge-coupled device (CCD) camera costing less than \$500 (CV S3200 Rev B, JAI, Japan) since one purpose of this study was to determine if one could use an inexpensive camera with a limited sensitivity and dynamic range to monitor optical changes in tissue. The camera is an analog video rate color CMY camera. The dynamic range of each channel is 8 bits. The camera CCD is sensitive to CMY colors; however, the camera transforms the measured CMY values into RGB values. The operation of the CCD camera was controlled using a PC computer and a LabVIEW program (National Instruments, Austin, TX). Figure 1(b) shows a photograph of the MDM system.

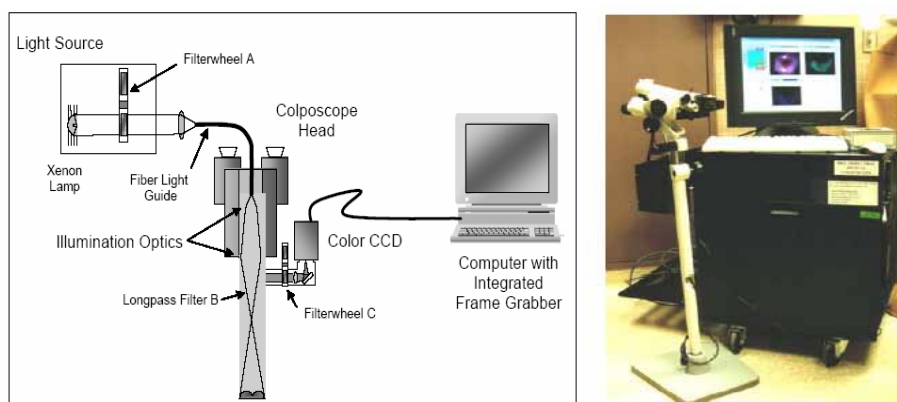


Fig. 1. (a) System diagram and (b) a photograph of the MDM system

2.2 Study design

Table 1 provides an overview of the study design. The protocol was reviewed and approved by the M.D. Anderson Cancer Center Animal Care and Use Committee. A laboratory animal veterinarian with extensive experience with the DMBA model of hamster cheek pouch carcinogenesis (LC) participated in all aspects of the study. Twelve animals were followed weekly for 16 weeks. Ten animals were treated with the carcinogen 0.5% DMBA in mineral oil to induce gradual epithelial carcinogenesis, and two control animals were treated only with mineral oil. Coghlan [4] showed that treating with DMBA more than two times per week results in acute inflammation and significant erosion in the early weeks of the protocol. Therefore, animals were initially treated with carcinogen two times per week starting in the second week of the study in order to allow the inflammation to subside; after six weeks, treatments were increased to three times per week since the acute inflammation in the early weeks ceased. Given the potency of DMBA, there is little difference in the overall average incidence of lesions at 16 weeks.

Table 1. Overview of the study design. DMBA weekly treatment frequency is indicated by the number in each cell; cells without a number indicate no DMBA treatment. Cells are color coded to indicate image acquisition and tissue classification. Different colors represent different tissue classifications: cyan for normal, green for intermediate, and red for neoplastic.

Animal No	Week															
	1	2	3	4	5	6	7	8	9	10	11	12	13	14	15	16
1																
2																
3		2	2	2	2	2	3	3	3	3	3	3	3	3	3	3
4		2	2	2	2	2	3	3	3	3	3	3	3	3	3	3
5		2	2	2	2	2	3	3	3	3	3	3	3	3	3	3
6		2	2	2	2	2	3	3	3	3	3	3	3	3	3	3
7		2	2	2	2	2	3	3	3	3	3	3	3	3	3	3
8		2	2	2	2	2	3	3	3	3	3	3	3	3	3	3
9		2	2	2	2	2	3	3	3	3	3	3	3	3	3	3
10		2	2	2	2	2	3	3	3	3	3	3	3	3	3	3
11		2	2	2	2	2	3	3	3	3	3	3	3	3	3	3
12		2	2	2	2											

In each treatment, the treatment substance was applied to the deepest recess of the right cheek pouch with a No. 5 camel-hair brush. Images of the treated cheek pouch were acquired weekly with the MDM, except for week 14. Prior to the measurement, animals were anesthetized with 75-150 mg/kg BW ketamine HCl (Fort Dodge, Overland Park, KS 66210) delivered intraperitoneally, and the pouch was rinsed with saline solution. In order to expose the deepest recess of the pouch, the hamster cheek pouch was manually everted with a gloved index finger of the handler. At image acquisition, the hamster was placed in a lateral recumbent position within the handler's gloved hand. The frame rate of the MDM is 30 frames/sec. Each white light image was taken at the full frame rate, while each fluorescence image was obtained by summing 32 fields, resulting in a frame rate of 1.875 frames/sec. The working distance of the MDM was 30 cm. The measured illumination intensity at this working distance was approximately 0.25 mW/cm² at 345 nm excitation and 2.4 mW/cm² at 440 nm excitation. Fluorescence was acquired sequentially at the two excitation wavelengths. Approximately one minute was required to obtain a sequence of reflectance and fluorescence images.

Based on the well-established natural history of the DMBA hamster cheek pouch model, the measured images were divided into three groups: normal, intermediate, and neoplastic. The normal group included images from the two control hamsters and those of DMBA treated hamsters measured in week 1 before application of carcinogen and in week 2. Images of DMBA treated hamsters after week 7 were assigned to the neoplastic group. Images of DMBA treated hamsters from week 3 to week 7 were classified into the intermediate group, since their disease progress could not be determined precisely without a biopsy.

2.3 Preprocessing and color transformation

White light and fluorescence images acquired from the hamster cheek pouches were preprocessed for three purposes: noise reduction, image registration, and correction for variations in the illumination intensity. Each animal was imaged at two different fluorescence excitation wavelengths; slight motion between image acquisition at the different excitation wavelengths necessitated proper image registration. The intensity of illumination varied from day to day, leading to variations in overall image intensity which were unrelated to the disease process. Image preprocessing included the following steps. First, median filtering was applied to each image to eliminate the fixed pattern noise due to the defective pixels in the CCD image sensor. Secondly, the two fluorescence images were aligned with the white light image. In this step, an automatic image registration algorithm based on mutual information was implemented to perform the image registration task without user intervention. Mutual information is a measure of the correlation of two images which is computed from the joint probability distribution of the two images' intensity. When two images are aligned, the resulting joint probability distribution of two images provides high-valued mutual information [22, 23]. Based on this property, white light and fluorescence images of the same object were aligned by maximizing the mutual information for each pair of these images. Finally, changes in the color and intensity of the image were separated using a color space transformation. Since the RGB color space is sensitive to both chromatic and intensity variations, images were transformed to the YCbCr color space, which achieves better color constancy [24]. The mathematical representation of this transformation [25] is provided in Eq. (1).

$$\begin{aligned}
 Y &= c_1R + c_2G + c_3B, \\
 C_b &= \frac{B - Y}{2 - 2c_3}, \\
 C_r &= \frac{R - Y}{2 - 2c_1},
 \end{aligned} \tag{1}$$

where $c_1 = 0.2989$, $c_2 = 0.5866$, and $c_3 = 0.1145$.

2.4 Feature selection and classification

Once images were transformed to the YCbCr color space, simple statistical features were examined to determine whether they provided useful diagnostic information. A previous study [4] showed increased fluorescence near 350-370 nm excitation and decreased fluorescence near 450-470 nm excitation associated with neoplasia. Based on this observation, the mean image intensity was selected as a potential feature for classification. As neoplasia progressed, we observed that the intensity variation across an image increased, therefore the standard deviation was explored as another potential feature for classification. The intensity distribution of the normal data set was much more similar to a Gaussian distribution than corresponding distribution of the neoplastic data set. A common statistic for assessing the normality of a distribution is the Jaque-Bera (JB) test statistic, which is determined by skewness and kurtosis of the data [26]. Based on this fact, skewness and kurtosis were also identified as potential features for image classification.

A classification algorithm was developed to discriminate images as normal or neoplastic. Input features include the mean image intensity in each channel at each excitation wavelength, the corresponding standard deviation of pixel intensity in each image channel at each excitation wavelength, skewness and kurtosis, for a total of 24 input parameters. The classifier is a linear discriminant algorithm based on the Mahalanobis distance measure.

The classifier was trained using images from the normal and neoplastic groups. For training purposes, an expert small animal veterinarian (LC) was asked to circle the neoplastic regions in the corresponding white light image for each animal in the neoplastic group. For each of normal group images, 2-3% of the pixels in the 345 nm and 440 nm excited fluorescence images were randomly selected; for each of the neoplastic group images, 2-3% of the pixels in the encircled neoplastic regions of the 345 nm and 440 nm excited fluorescence images were randomly selected. The random sampling was performed using the uniform distribution. The statistical features associated with these randomly chosen pixels were used to train the classifier to identify tissue as normal or neoplastic. This random sampling technique was applied in order to reduce the likelihood of overtraining and to increase the robustness of the algorithm. The algorithm was trained using data from all but one hamster in the normal and neoplastic groups. This algorithm was then applied to data from the held-out animal and to animals from the intermediate group. In applying the algorithm, 2-3% of the pixels from the 345 nm and 440 nm excited fluorescence images were randomly chosen as input to the classifier without regard for the location of the areas encircled by the expert veterinarian. This process was repeated until all hamster images from the normal, intermediate and neoplastic groups had been classified. Note that the classification results for the intermediate group provided additional information on diagnostic features even though they were not utilized when the quantitative diagnostic performance measures such as sensitivity and specificity were evaluated.

3. Results

Figure 2 shows a time course of white light and autofluorescence RGB images of the DMBA treated cheek pouch of hamster 10. Fluorescence intensity changes associated with the dysplasia to carcinoma sequence can be clearly seen in Fig. 2(b)-(e). The images in Fig. 2 are representative of those obtained in the study. The left column shows the white light images. In each white light image, abnormal areas identified by the expert veterinarian are enclosed with a green line. The middle and right columns show fluorescence images acquired at 345 nm and 440 nm excitation, respectively. Images obtained in week 1, before application of carcinogen, serve as base line images for comparison with those in weeks 5, 7, 11, and 13. In week 5, a dysplastic lesion was observed. By week 7, a small exophytic neoplastic lesion has formed. These lesions progress to an obvious neoplasm in week 11. Consistent with human neoplasms, the malignant tumor in week 13 has begun outgrowing its blood supply and appears necrotic. At 345 nm excitation, dysplasia and tumor appear brighter than the surrounding normal tissue. However, the necrotic tumor at week 13 appears dark. At 440 nm excitation, the dysplasia looks lighter green. As the tumor appears and progresses, red fluorescence is observed in the images (Fig. 2(c)-(e)). However, as shown in Fig. 2(e), we consistently observed a decrease in the red fluorescence decreased when the malignant tumor formed in all DMBA treated hamsters.

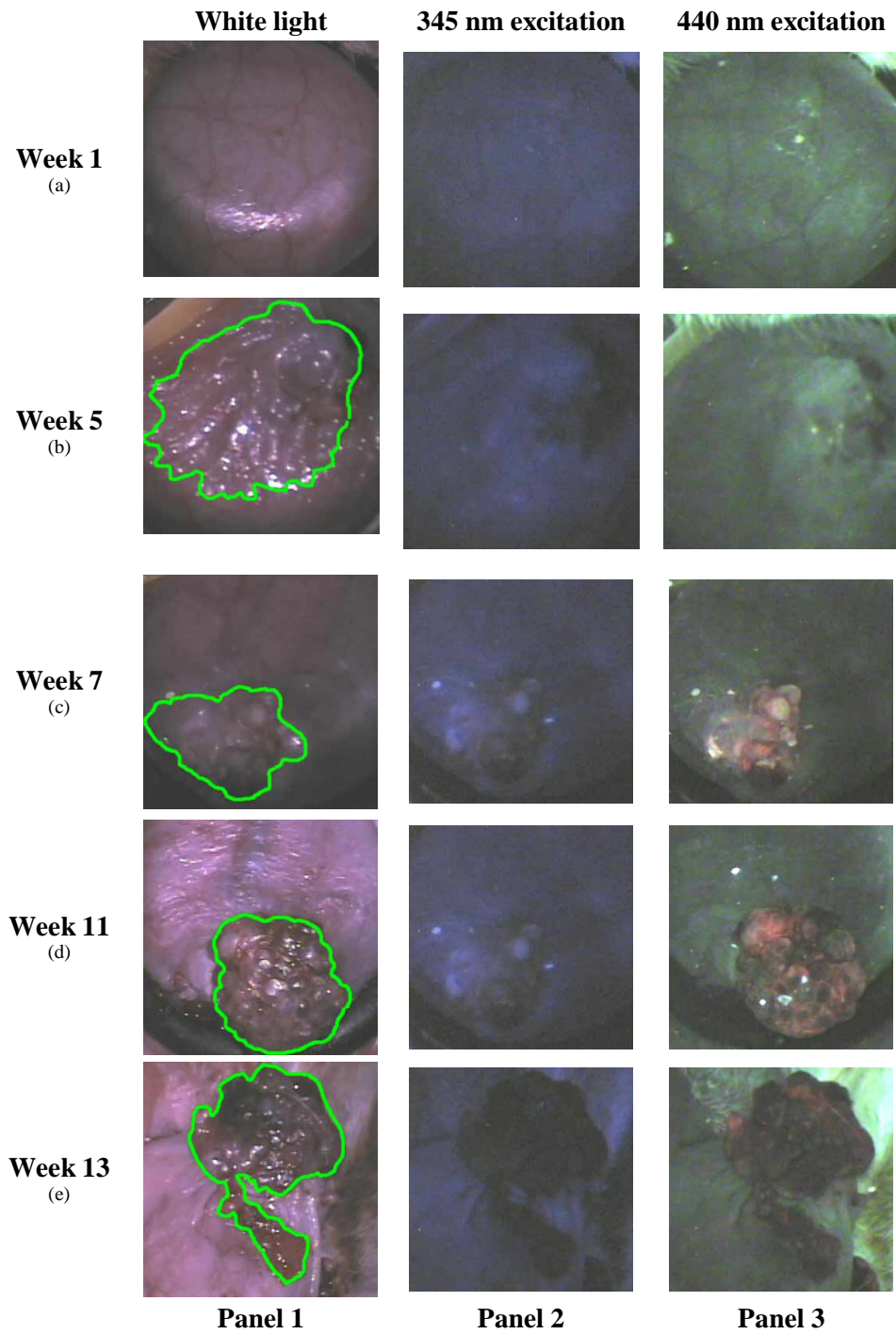


Fig. 2. Time course of RGB images for a representative DMBA treated hamster : 1st week, b) 5th week, c) 7th week d) 11th week, and e) 13th week (left: white light reflectance images, middle: 345 nm excited fluorescence images and right: 440 nm excited autofluorescence images).

Figure 3 shows relative frequency histograms of the parameters extracted from pixels randomly chosen from images in the normal and neoplastic groups. Figure 3(a) shows histograms of the mean intensity in the three color channels from the pixels randomly chosen from the normal and neoplastic group images in the RGB color space. Figure 3(a) shows histograms of the mean fluorescence intensity at 345 nm excitation for the red (left), green (middle), and blue (right) color channels. Figure 3(b) shows similar plots for the pixels from images acquired at 440 nm excitation. At both 345 nm and 440 nm excitation, the histogram of the mean intensity of the pixels of images from the abnormal hamsters is asymmetric and shifted to lower values, while that from the normal hamsters is fairly symmetric and shifted to higher values.

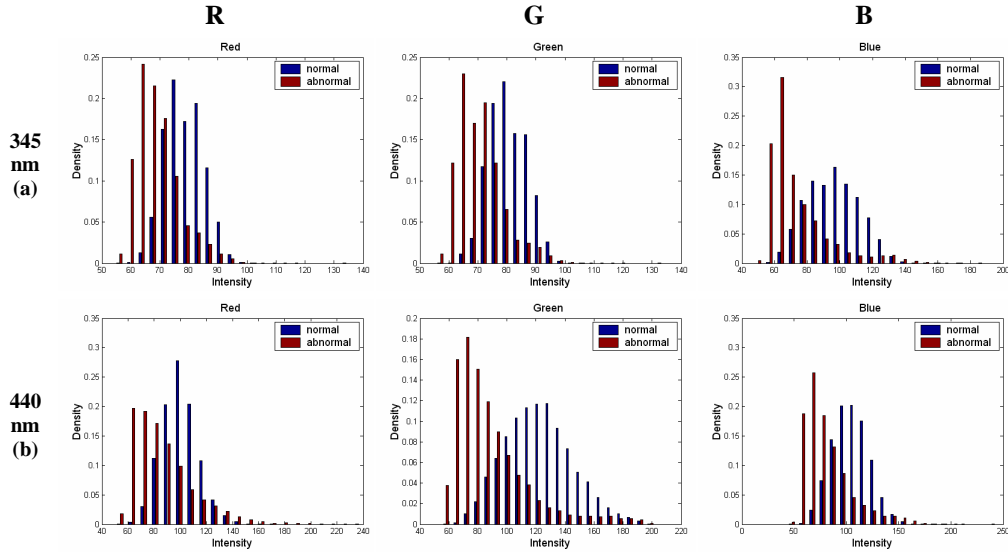


Fig. 3. Relative frequency histograms of the mean intensity of pixels randomly chosen from fluorescence images at (a) 345 nm and (b) 440 nm excitation in the normal and neoplastic groups. The left column shows data from the red channel, the middle column from the green channel and the right column from the blue channel.

Figures 4(a), (b), (c) and (d) show scatter plots of the mean, the standard deviation, the skewness, and the kurtosis, respectively, of the intensity at 345 nm excitation versus values at 440 nm excitation for each hamster at each time point in the normal, intermediate and neoplastic groups. Results are shown for each of the red, green, and blue channels. A noticeable separation between the normal and the neoplastic data can be observed in the mean intensity plots for the red, green, and blue channels. Interestingly, the mean intensities from images in the intermediate group are clustered in between those of the normal and neoplastic groups. The intermediate group represents a transition from normal to dysplasia, suggesting that the mean intensity feature changes continuously as neoplasia progresses. However, the other statistical measures do not show any clear separation in this color space. Using these RGB parameters as input, a linear discriminant classifier based on the Mahalanobis distance measure was applied; images from the normal and neoplastic groups were classified with a sensitivity of 84% and a specificity of 79%.

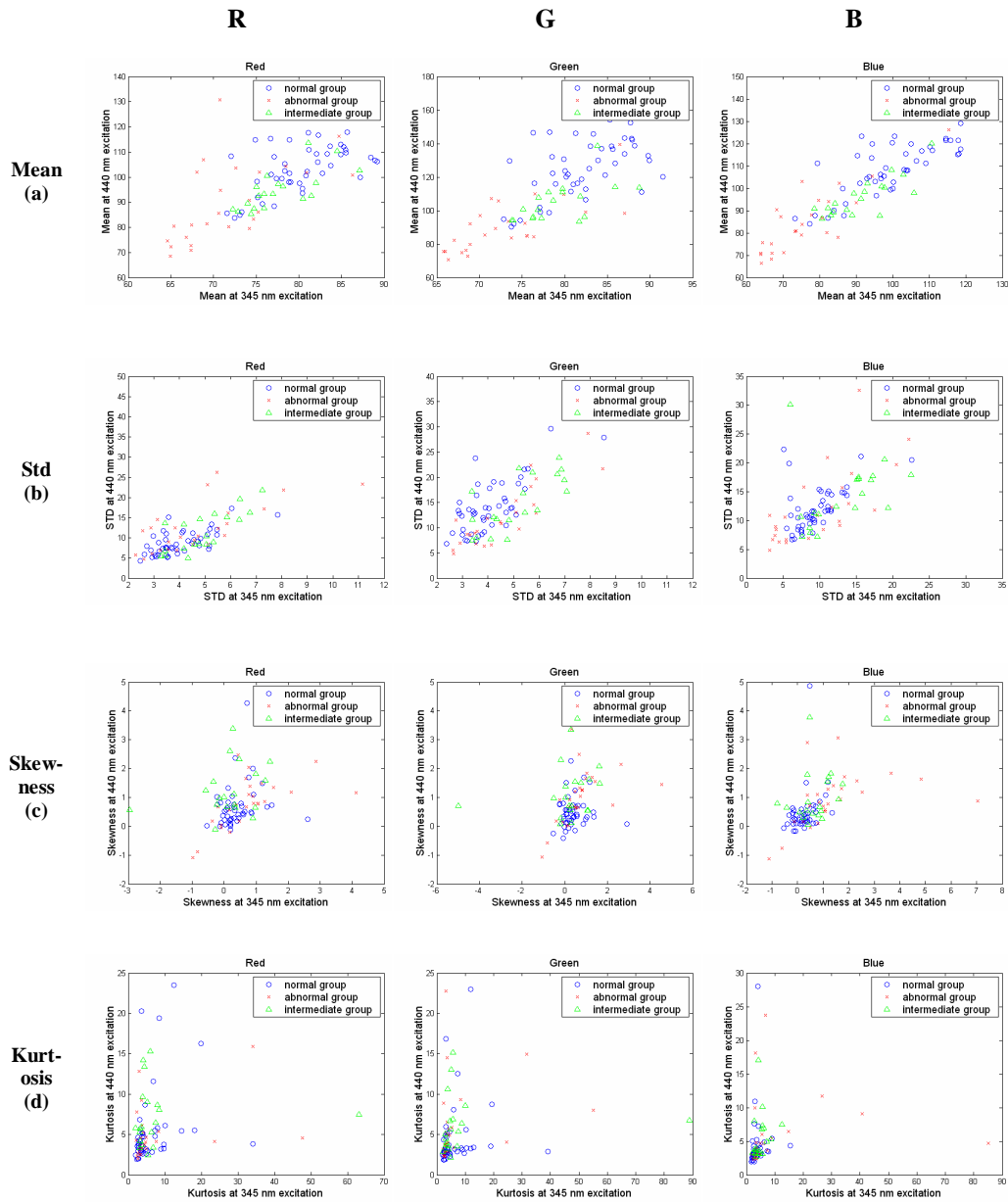


Fig. 4. Two dimensional scatter plots of the statistical parameters from pixels randomly chosen from fluorescence images at 345 nm excitation vs the same parameters at 440 nm excitation, including (a) mean intensity, (b) standard deviation, (c) skewness and (d) kurtosis. The left column shows data from the red channel, the middle column from the green channel and the right column from the blue channel. A data point is shown for each hamster at each time point in the normal, intermediate and neoplastic groups.

Figure 5 shows similar relative frequency histograms for the mean intensity, standard deviation, skewness and kurtosis in the YCbCr color space of pixels randomly chosen from images in the normal and neoplastic groups. Figure 5(a) shows the mean intensity histograms at 345 nm excitation for the Y (left), Cb (middle), and Cr (right) channels. Figure 5(b) shows the mean intensity histograms plots at 440 nm excitation. At 345 nm excitation, the mean intensity histograms of the neoplastic group are asymmetric and shifted to lower values in both the Y and Cb channels, while that in Cr channel is shifted to higher values. At 440 nm excitation, the mean intensity distribution in the Y channel is asymmetric and shifted to lower values in the neoplastic group, while slightly asymmetric and shifted to higher values in both the Cb and Cr channels,. At both excitation wavelength and for all three channels, the mean intensity distributions of the normal hamsters are symmetric.

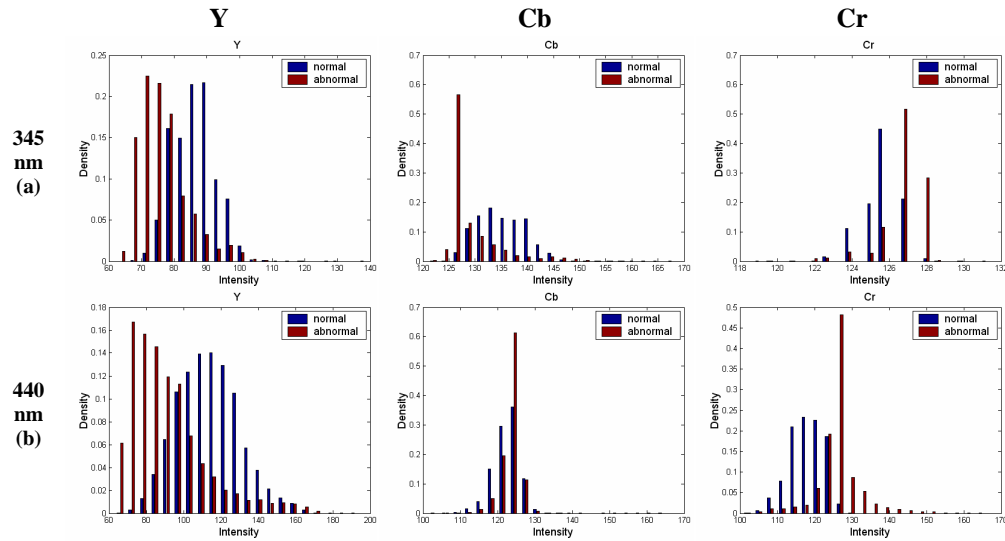


Fig. 5. Relative frequency histograms of the mean intensity of pixels randomly chosen from fluorescence images at (a) 345 nm and (b) 440 nm excitation in the normal and neoplastic groups. The left column shows data from the Y channel, the middle column from the Cb channel and the right column from the Cr channel.

Figures 6(a), (b), (c) and (d) show two dimensional scatter plots of the mean, the standard deviation, the skewness, and the kurtosis of the intensity at 345 nm excitation versus those at 440 nm excitation, respectively, for each hamster at each time point in the normal, intermediate and neoplastic groups for each of the Y, Cb, and Cr channels. Clear separation between the normal and the neoplastic data is observed in both the Cb and Cr channels for all statistical parameters except kurtosis. In the Y channel, no clear separation is observed for any of the statistical measures. Using these YCbCr parameters as input, a linear discriminant classifier based on the Mahalanobis distance measure was applied; images from the normal and neoplastic groups were classified with a sensitivity of 96% and a specificity of 84%.

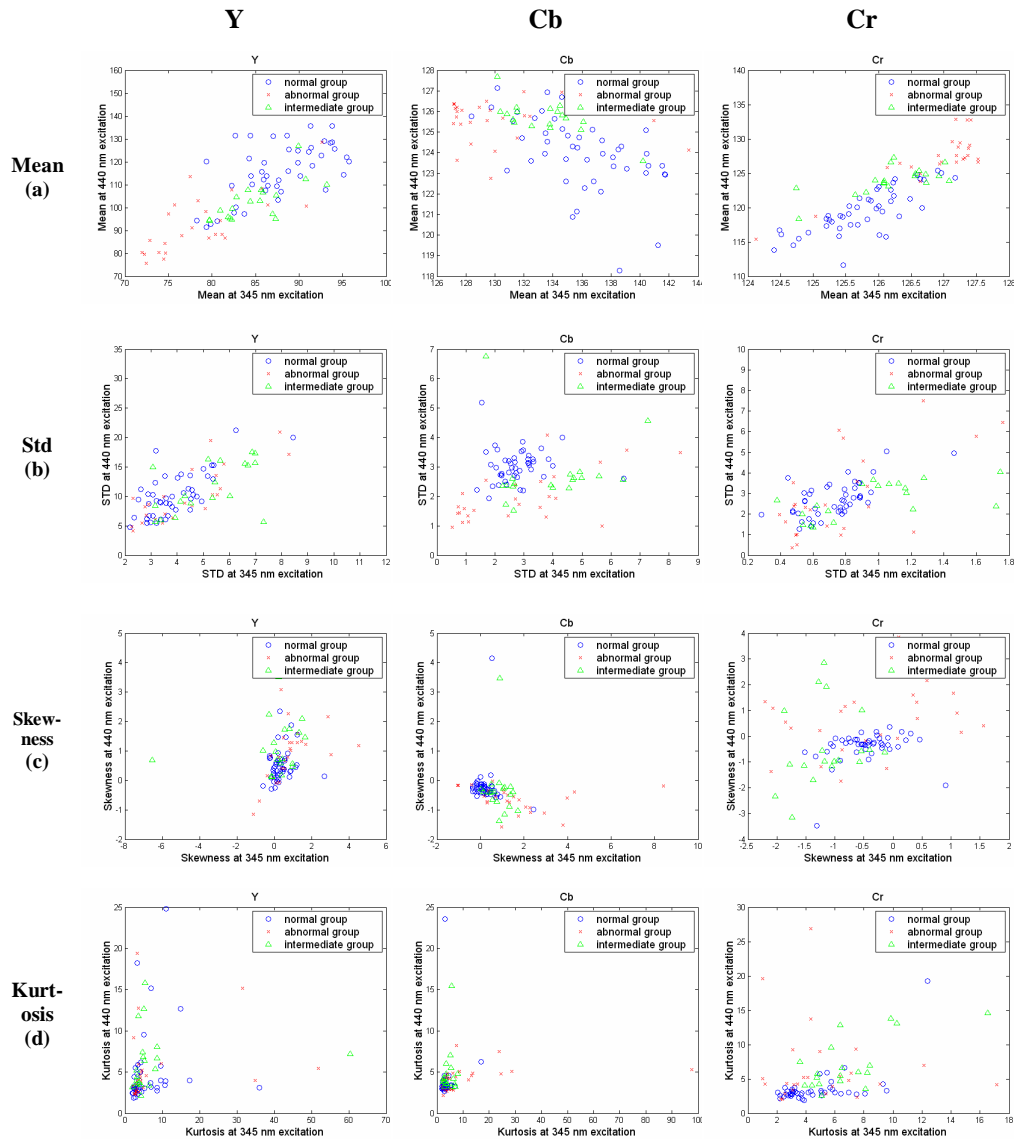


Fig. 6. Two dimensional scatter plots of the statistical parameters from pixels randomly chosen from fluorescence images at 345 nm excitation vs the same parameters at 440 nm excitation, including (a) mean intensity, (b) standard deviation, (c) skewness and (d) kurtosis. The left column shows data from the Y channel, the middle column from the Cb channel and the right column from the Cr channel. A data point is shown for each hamster at each time point in the normal, intermediate and neoplastic groups.

Table 2 presents the detailed results of the classification algorithm applied to images in the YCbCr color space for each hamster at each time point. Only one image from the neoplastic group was misclassified. Although the images from the intermediate group were not included in the calculation of sensitivity and specificity, it is interesting to examine the classification results for this group. Most of the images in this category were classified as abnormal. Furthermore, for all but one hamster, once data from an animal was classified as abnormal, the images at subsequent time points were also classified as abnormal.

Table 2. Classification results using the input data from images in the YCbCr color space for each hamster at each time point. Colored cells indicate time points at which images were acquired. The cells are color-coded to indicate which group the images were assigned to as in Table 1. The results of the classification algorithm are represented by the letter in the cell, where N indicates the measurement was classified as normal and A indicates the measurement was classified as neoplastic. Circled letters indicate misclassifications for hamsters in the normal and neoplastic groups.

Animal No	Week															
	1	2	3	4	5	6	7	8	9	10	11	12	13	14	15	16
1	N	N	N	N	N	N	A	N	(A)	N	N	N	N		N	N
2	N	N	(A)	N	N	N	N	N	N	(A)	N	N	N		N	N
3	N															
4	N			A		N		A		A		A				A
5	N	(A)		A		A		A		A		A				A
6	N	N		N		A		A		A		A				A
7	(A)	(A)		A		A		A				A				A
8	N	(A)		A						A					A	
9	N		A		A						A		A			
10	N		A		A		A		A		A		A			
11	N		N		N		A		A		A		(N)		A	
12	N		A		A											

4. Discussion

Compared to point spectroscopy, the multispectral imaging with the MDM has the advantage of providing a real time assessment of the entire field at risk. In this study, we show that a simple analysis extracting image features such as the mean image intensity or standard deviation can yield diagnostic performance which is similar to that of point spectroscopy [4]. Best results are obtained when the images are represented in the YCbCr color space, enabling good separation of intensity and chromatic changes. In particular, moving to the YCbCr color space simplifies the ability to monitor the increase in red fluorescence associated with neoplasia at 440 nm excitation. This observation has been reported in previous spectroscopy studies, and is attributed to porphyrin fluorescence. The origin of this porphyrin fluorescence is controversial and whether it is associated with tumor cells or with microbial contamination is unclear [27]. In the RGB color space, due to the high correlation of all three RGB color channels with intensity variations [24], the changes in red fluorescence are mingled with changes in overall intensity. In the YCbCr color space, the intensity variations are clearly separated from changes in chromatic features. Earlier studies with point spectroscopy indicate that the presence of red fluorescence is associated with neoplasia, but is not always present. In this study, an increase in red fluorescence was consistently observed at 440 nm excitation near the neoplastic lesions for all the DMBA treated hamsters. However, the red fluorescence was heterogeneously distributed, and studies with point spectroscopy that interrogate only a small point on the tissue may not adequately sample the lesion. The MDM provides a more holistic assessment of the field at risk. In the future, it may be possible to further improve diagnostic performance by exploring spatial variations in statistical parameters throughout the image.

A potential weakness of this study is that a confirmatory biopsy was not obtained at each time point. While it would provide definitive diagnostic information, such frequent biopsies would clearly suppress the development of neoplasia and would significantly alter the natural history of the lesions. Since the hamster cheek pouch model is so well-characterized with clear time points at which neoplasia develops, the use of the model with the lack of biopsies was adopted rather than performing frequent biopsies. In summary, the MDM provides an inexpensive tool to monitor changes in the autofluorescence associated with neoplasia. Use of such an inexpensive system may prove useful for improved cancer screening in regions with limited health care resources. Clinical applications of this technique may include improved early detection, better direction of diagnostic biopsy and real time determination of tumor margins.

Acknowledgments

We thank Dr. Irma Gimenez-Conti in histopathology & immunohistochemistry for processing and consultation on this work. Financial support by the University of Texas M.D. Anderson Cancer Center Support Grant (CA166672) and the NIH-NCI Program Project Grant (2PO1CA082710-06) is gratefully acknowledged.